Biomed Microdevices
DOI 10.1007/s10544-014-9853-5

Optical biosensors with an integrated Mach-Zehnder Interferometer for detection of *Listeria monocytogenes*

Dibyo Sarkar · Naga Siva Kumar Gunda · Iqbal Jamal · Sushanta K. Mitra

Abstract In this work, we have demonstrated an efficient optical immunoassay technique for the detection of a food-borne pathogen, *Listeria monocytogenes*, using a Mach-Zehnder Interferometer (MZI) configuration. We have investigated ten different MZI configurations with angular and Sbend Y-junction geometries. An efficient Hydrofluoric acid (HF) based technique was used for rapid and specific binding of *L. monocytogenes* to the sensor arm of the MZI biosensor. The MZI biosensor was able to detect *L. monocytogenes* at concentrations of the order of 10^5 CFU/ml, which is lower than the infection dose for healthy human beings. SEM analysis and light intensity measurements showed the biosensor is highly selective to *L. monocytogenes* over other microbial species (such as *Escherichia coli*). Finally, a novel calibration scheme of the MZI biosensor was developed from experimental data that can be used for determining unknown concentrations of *L. monocytogenes*.

Keywords Biosensor · Fabrication · Biofunctionalization · Selectivity · Limit of detection · Scanning electron microscope

D. Sarkar · N. S. K. Gunda · S. K. Mitra (✉)
Department of Mechanical Engineering, University of Alberta, Edmonton, T6G 2G8, Canada
e-mail: sushanta.mitra@ualberta.ca

I. Jamal
AQL Management Consulting Inc., 4216 109A St NW, Edmonton, AB, T6J 2R8, Canada

1 Introduction

Listeria monocytogenes is a pathogen found in soil, water, and vegetation that can grow in refrigeration temperatures and can pose a threat to human health. *L. monocytogenes* is a gram-positive, rod-shaped food-borne pathogen that causes listeriosis, which can have a high mortality rate (25–30 %) in immune-compromised populations (Aureli et al. 2000; Frye et al. 2002) and pregnant women (Donnelly 2001; MacDonald et al. 2001). Previously, *L. monocytogenes* outbreaks were mainly reported in seafoods (Embarek 1994) but the recent outbreaks in ready-to-eat (RTE) meat products (Donnelly 2001; Schlech and Acheson 2000) have increased the need for more rapid, sensitive, and selective methods for detection of this bacterium in RTE products. In this paper, we demonstrate an efficient optical immunoassay technique for the detection of *L. monocytogenes*.

Traditionally, the detection of *Listeria* is conducted by culture-based methods, which are time consuming and often labor intensive. Typically, four sequential steps are required for culture-based methods of detection—pre-enrichment, selective enrichment, selective plating, and biochemical screening (Chin et al. 2007). The incubation periods can range from several weeks to months, a time frame over which the contaminated RTE meat products would have left the processing plant and already been available to consumers in grocery stores.

Currently, the detection methods for *L. monocytogenes* that are commercially available are assay based, which include enzyme-linked immunosorbent assay (ELISA) (Mattingly et al. 1987), enzyme-linked immunofluorescence assay (ELFA) (Ueda and Kuwabara 2010; Sewell et al. 2003), fluorescence *in-situ* hybridization (FISH) (Fuchizawa et al. 2009; Almeida et al. 2011; Moreno et al. 2011), and polymerase chain reaction (PCR) (Omiccioli

Published online: 26 March 2014

et al. 2009; Kim and Cho 2010; Traunšek et al. 2011; Pochop et al. 2012; Kotzekidou 2013; Shu et al. 2013). Most of these methods need selective enrichment for up to 48 h. These techniques are laboratory based and are not applicable for real-time identification of *L. monocytogenes* in the field. They also require the use of large quantities of expensive samples and reagents, and trained personnel. Hence, there is a real need to develop a technology that will allow rapid, sensitive and cost-effective identification of *Listeria monocytogenes* in food samples.

The use of biosensors for detection of biomolecules has seen rapid progress in the last two decades. Integration of sensors with microelectronics and wireless communication provides high sensitivity, rapid analysis and allows real-time monitoring. Their compatibility with Integrated Circuit (IC) fabrication technologies allows for low-cost large scale fabrication, thus indicating a promising future of biosensors for rapid detection platform. Biosensors use various techniques for the detection of analytes (Griffiths and Hall 1993; Ivnitski et al. 1999; Leonard et al. 2003; Su et al. 2011), of which label-free optical biosensing technique is widely used due to its simplicity in fabrication, portability, small footprint, low-cost, real-time detection, and high sensitivity (Marazuela and Moreno-Bondi 2002; Fan et al. 2008).

In this work, a Mach-Zehnder Interferometer (MZI) monomode waveguide based on total internal reflection (TIR) has been used for label-free optical detection of *Listeria monocytogenes*. The use of MZIs as optical biosensors is rapidly progressing (Esinenco et al. 2005; Müller et al. 2005; Sepulveda et al. 2006; Zinoviev et al. 2008; Bruck et al. 2011) since its first inception by Heideman et al. (1993). In the MZI device, a light beam propagating within the monomodal waveguide is divided into two identical arms (refer Fig. 1), the sensor and the reference arms, by means of a Y-junction. After traveling a certain distance (L), the light beam converges, by means of another Y-junction, creating an interference signal. In the sensor arm, a specific area (sensor area) is etched where an electromagnetic field of the propagating light waves, called the evanescent field, can interact with analytes (Brosinger et al. 1997; Parriaux and Veldhuis 1998; Rohrbach 2000; Marazuela and Moreno-Bondi 2002). This interaction causes a change in the effective refractive index of the sensor arm, which will induce a phase difference between the light beams traveling in both arms. This phase difference will depend on the difference of the effective refractive indices of the sensor and the reference arms and on the interaction length (S_l as in Fig. 1) of the sensor area.

In a recent work reported by Sarkar et al. (2013), they have demonstrated a systematic approach for the design and fabrication of MZI biosensors with minimum power loss. In their work, they have performed a detailed theoretical and numerical analysis of light field propagation in an MZI waveguide and have quantified the dimensional constraints required for low-loss MZI designs. They have successfully fabricated and tested these low-loss MZI chips showing excellent match between experimental and simulated power losses. The work presented here involves using the fabricated MZI chips reported in (Sarkar et al. 2013) with the entire chip size as small as 1.5 mm by 30 mm; biofunctionalization of *L. monocytogenes* on the sensor area using a covalent immobilization technique; detection of phase change in the sensor and reference arms through power measurements; determination of limit of detection (LOD) and range of detection (ROD) of the biosensor, and selectivity with respect to other species of bacteria. The novelty of this work is as follows: a biosensor, highly selective to *Listeria*, has been developed and successfully tested; a new immobilization technique used here has shown highly specific binding of *Listeria* to the sensor area and reduction of the biosensing time; capillary force has been used instead of pumps as a means to transport the biomolecules into the sensor area making the entire system independent of an external power source; and for the first time, an MZI biosensor has been calibrated, using phase change data, which can be used to determine unknown concentrations of bacterial solutions.

2 Materials and methods

2.1 Chemicals and materials

Four inch prime grade polished Silicon wafers were purchased from NanoFab at the University of Alberta, Edmonton, AB. 48 % aqueous Hydrofluoric acid (HF) and Sodium bicarbonate ($NaHCO_3$) were obtained from the Chemistry Department at the University of Alberta. Glutaraldehyde (50 % aqueous solution), phosphate buffer solution (PBS), 2-aminoethanol or ethanolamine (≥99.5 %), isopropanol and ethanol were purchased from Sigma Aldrich, Canada. Freeze-dried *L. monocytogenes* (ATCC strain 43251), unconjugated and FITC tagged rabbit anti-*L. monocytogenes* were provided by Cedarlane®, Burlington, ON, Canada. All solvents used were reagent grade and deionized water (DI-H_2O) was used throughout.

2.2 Techniques used

Fabrication of the MZI chips was performed in the NanoFab facility at the University of Alberta, Canada. Characterization of the fabricated chips was carried out using atomic force microscopy (AFM) and ellipsometry. AFM (MFP-3D, Asylum Research, Santa Barbara, CA, USA) was used to measure the dimensions of the fabricated MZI chip. Ellipsometric measurements were used to determine the thickness

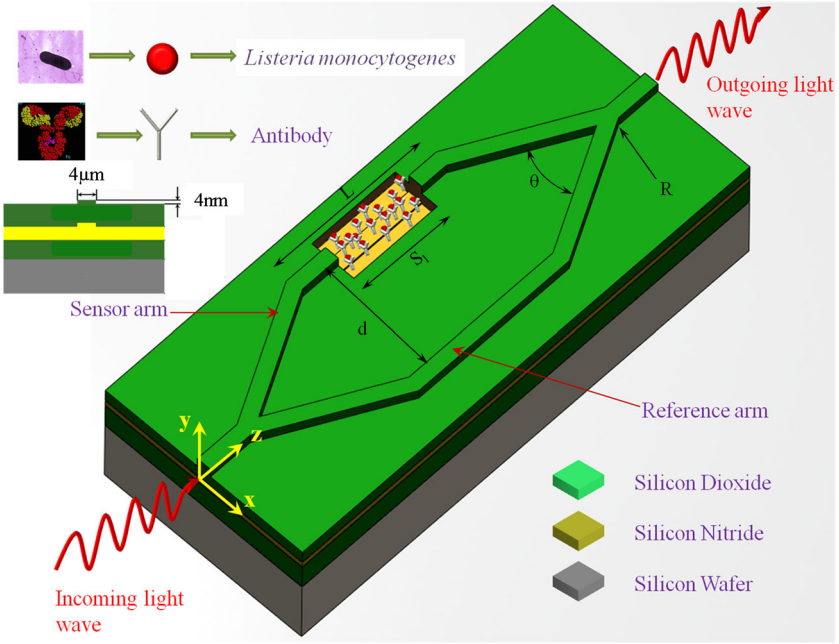

Fig. 1 Schematic representation of biofunctionalization on MZI. Here, S_l is the length of the sensor area, L is the length of the sensor arm, d is the distance between the sensor and reference arms and θ is the opening angle of the Y-divisor for angular Y-junctions, whereas R is the radius of curvature of the Y-divisor for Sbend Y-junctions

and refractive index of each layer of the chip using a Sopra GES5E Spectroscopic Ellipsometer (France).

Fluorescent microscopy and scanning electron microscopy (SEM) were used for qualitative study of *L. monocytogenes* functionalization on the chip surface. An inverted fluorescent microscope (Leica DMI6000, Leica Microsystems Inc., ON, Canada) was used to determine the presence of bacteria only on a certain area of the chip (sensor area). SEM (LEO 1430, ZEISS, Germany) was used for imaging the MZI chips to confirm the selectivity of the chip for a given species of the bacteria (*L. monocytogenes*).

Contact angle measurements were performed using a Krüss Drop Shape Analysis System DSA100 (Germany). All measurements were done at room temperature and the values reported are the averages of four separate drops on a given surface.

3 Experimental procedure

3.1 Fabrication of MZI chips

The MZI chips were fabricated using nine major steps. The details of the fabrication procedure is already reported elsewhere (Sarkar et al. 2013). A brief summary of the entire procedure is presented here. The general structure, as shown in Fig. 1, consists of a silicon substrate $< 100 >$, a 1.5 μm thick layer of thermally grown SiO_2 acting as the lower cladding whereas a 2 μm thick layer of chemically deposited (plasma enhanced chemical vapour deposition or PECVD) SiO_2 forms the upper cladding layer. These two layers sandwich a 250 nm Si_3N_4 core layer deposited by low pressure chemical vapour deposition (LPCVD). The core and cladding layers have a refractive index of 2 and 1.46, respectively, which is ideally suited for total internal reflection (TIR) in a monomode waveguide (Heideman and Lambeck 1999; Pal, 1992). The MZI configuration was printed on the core layer in the form of a 4 μm $\times$ 4 nm ridge structure by a standard photolithographic and reactive ion etching (RIE) technique. Finally, a sensor area was formed by etching through the upper cladding SiO_2 layer (2 μm deep, 100 μm wide and a varying length, S_l) over a certain area on one of the MZI arms (also called the sensor arm), as shown in Fig. 1. The entire length and width of the chip is 30 mm and 1.5 mm, respectively. Figure 2 shows the SEM image of the 2 μm deep and 100 μm wide cavity, which represents the sensor area. The SEM image provides

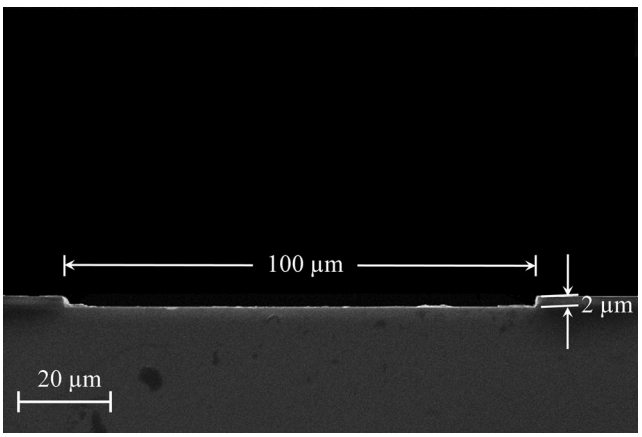

Fig. 2 SEM image of cross-section of sensing area of the fabricated MZI chip

the cross-sectional area of the MZI chip over which the biofunctionalization will take place. The entire procedure of fabricating the MZI chip is summarized in Fig. 3.

Based on the theoretical analysis of the design of MZI structures (Sarkar et al. 2013), ten different MZI configurations were fabricated. These ten different chips can be classified into two broad categories: Angular and Sbend, depending on the shape of the Y-junction divisors of the MZI. The angular MZI is formed with Y-junctions having an opening angle denoted by θ, whereas the Sbend MZI is formed with Y-junctions having circular bends with radii denoted by R. The column 1 of Table 1 represents the two different configurations, where A represents the angular Y-junctions and S represents the Sbend Y-junctions. Column 2 represents the opening angle (θ) for angular Y-junctions and radius of curvature (R) for Sbend Y-junctions. The columns 3 and 4 represent the distance between the two arms (d) and length of the arms (L), respectively. The θ values are kept below a certain critical angle ($<2.5°$) and the R values kept above a certain critical radius (>15 mm) to ensure that the optical losses incurred in the waveguide are with acceptable limits (Sarkar et al. 2013). The columns 5 and 6 represent the length (S_l) and surface area (A_s) of the sensor area, respectively. The last column gives the optical losses for each type of chip, in terms of dB/cm when light from a laser source propagates through them, as measured by a photodiode. For the same sensing length S_l, losses incurred in the Sbend Y-junction designs were much lower than their angular Y-junction counterparts. This can be attributed to the more gradual wave guiding approach of the Sbend design.

There are two deciding factors when it comes to selecting an MZI design for biosensing, namely (i) the optical losses and (ii) the area of sensing. From Table 1, it can be clearly seen that $S1$ ($R = 180$ mm) is the best design in terms of lowest optical losses. However, the area of sensing is quite low compared to other designs (1 mm^2). For high sensitivity biosensing experiments, an optimal design is required which would have a larger sensing area with low optical losses. Hence, for the experiments performed in the present work, the $S3$ design of the Sbend configuration was chosen. It has a large sensing area (50 % greater than $S1$) yet has an acceptable level of optical losses (0.4 dB/cm).

3.2 Immobilization of *L. monocytogenes* on the sensor area

An immobilization protocol was developed in our laboratory (Micro & Nano-scale Transport Laboratory, University of Alberta) to selectively bind the bacterial cells to the sensor area of the MZI chip only. Silicon dioxide covers almost 97 % area of the chip surface with only 3 % being the silicon nitride sensor area. Therefore, a procedure was required to create more affinity of *L. monocytogenes* towards the silicon nitride surface (open sensor area) as compared to the silicon dioxide surface (rest of the chip area). This was achieved by the following steps, outlined here.

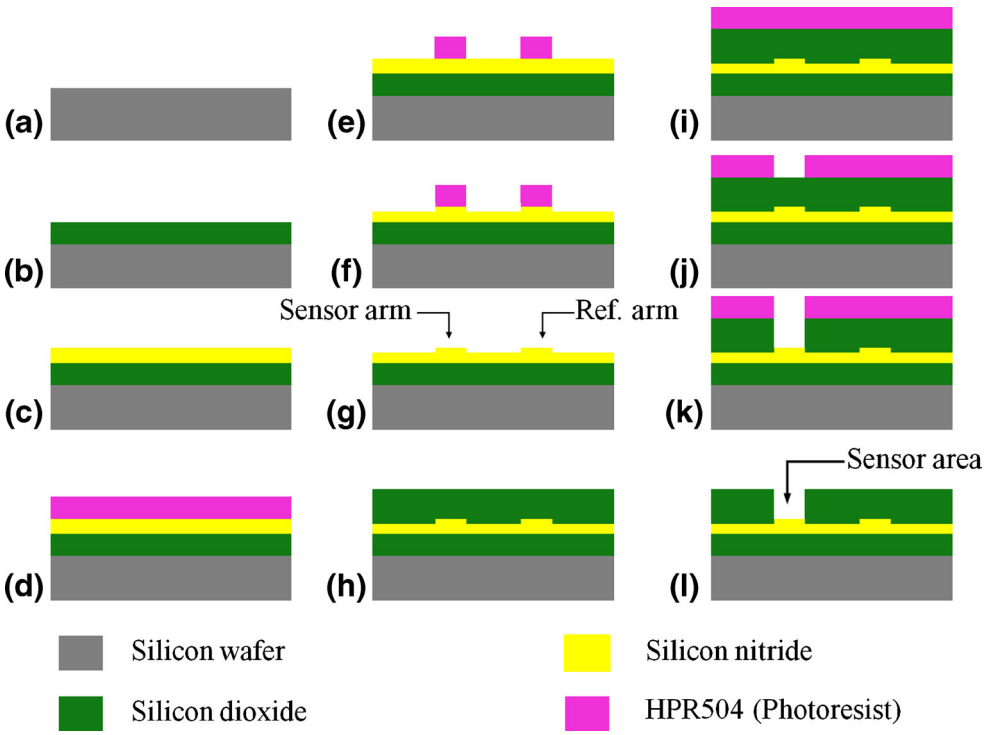

Fig. 3 Schematic of the fabrication procedure at cross-section of the chip. It involves **a** bare silicon wafer, **b** thermal oxidation of silicon dioxide on the silicon wafer forming the lower cladding, **c** LPCVD of silicon nitride core layer, **d** photoresist (HPR504) spinning on the silicon nitride layer, **e** photolithography defining the MZI configuration, **f** RIE of 4nm depth printing the MZI configuration, **g** resist stripped revealing the sensor and reference arms, **h** PECVD of silicon dioxide forming the upper cladding, **i** HPR504 photoresist spinning on the silicon dioxide layer, **j** photolithography defining the sensor area, **k** RIE of upper cladding creating the sensing area and **l** resist stripped revealing the entire MZI biosensor chip

Table 1 Different configurations of the fabricated MZI chips

Y-junction design	$\theta(deg)$ for angular/ R(mm) for Sbend	Distance d (μm)	Length of arm $L(\mu m)$	Length of sensor area S_l(mm)	Surface area of sensor area A_s(mm^2)	Propagation losses (db/cm)
Angular						
A1	0.9	80	16	12	1.2	0.40
A2	1	100	14	10	1.0	0.50
A3	2	100	20	15	1.5	0.72
A4	2	80	21	15	1.5	0.72
A5	2.5	80	22	16	1.6	0.88
Sbend						
S1	180	100	14	10	1.0	0.28
S2	150	80	16	12	1.2	0.36
S3	56	80	20	15	1.5	0.40
S4	25	80	22	16	1.6	0.62
S5	20	100	22	16	1.6	0.69

3.2.1 HF treatment

The fabricated MZI chips were cleaned in a piranha solution (3 parts H_2SO_4 and 1 part H_2O_2) for 15 mins to remove all the organic impurities from the surface. Following that, the chips were rinsed in DI-H_2O and blow-dried with a nitrogen gun. Then, the chips were dipped in a 1 % HF solution for 3 minutes and rinsed thoroughly with DI-H_2O. The piranha cleaning creates a native oxide layer on the silicon nitride surface (Menon and Donovan, 1993) which is removed by the HF treatment (Williams and Muller 1996; Bañuls et al. 2010).

3.2.2 Modification of surface with glutaraldehyde

The HF treatment performed in the previous step also enhances the concentration of amine (N-H) groups on the Si_3N_4 surface (Cattaruzza et al. 2004; Karymov et al. 1995). The freshly treated chips were then immediately immersed in a 5 % glutaraldehyde solution for 90 mins in a nitrogen atmosphere at room temperature. During this step, glutaraldehyde reacts with the amine groups (present only on the silicon nitride surface) generating aldehyde groups. The chips are then washed thoroughly in DI-H_2O and PBS before drying them with a nitrogen gun.

Contact angle measurements, performed on silicon nitride surface, showed an increase in water contact angle from $30 \pm 2°$ to $48 \pm 4°$ (refer Fig. 4a) after being treated with glutaraldehyde whereas silicon dioxide surface treated with glutaraldehyde following a similar protocol showed an unaltered value for the contact angle ($18 \pm 1°$) (refer Fig. 4b). This indicates that the glutaraldehyde crosslinkers are anchored exclusively to the amine groups of the silicon nitride (sensor area) portion of the chip.

3.2.3 Immobilization of L. monocytogenes

Unconjugated rabbit anti-*L. monocytogenes* antibody (0.1 mg/ml) was added to the glutaraldehyde treated chips and incubated for 30 mins at room temperature. During this period, the aldehyde groups covalently bond with the primary amine of the antibodies. After this period, to prevent any unspecific binding, the unbound aldehyde groups were blocked with 0.1 M ethanolamine for 15 mins at room temperature. The MZI chips were then incubated for 30 mins with increasing concentrations of *L. monocytogenes* in brain heart infusion (BHI) broth solutions (2.8×10^3 CFU/ml to 2.8×10^{13} CFU/ml). Finally, the chips were rinsed with PBS and DI water and blown dry with nitrogen. The schematic representation of surface modification and immobilization is shown in Fig. 5.

The initial concentration has been estimated based on the sensor area and approximate antibody dimension to create an antibody monolayer. We used the initial concentration as 0.1 mg/ml, which is more than the sufficient concentration to create the monolayer of antibody on sensor area. The present study uses S3 configured MZI chips (optimized design) to demonstrate the detection of listeria. The sensor surface area of S3 configured MZI chip is 1.5 mm^2. By considering approximate dimension of listeria antibody as 7.5 nm diameter, the surface area required for each antibody is calculated as 44.18 nm^2. From this approx. area of antibody, the number of antibodies required to cover the sensor surface area is determined and it is found that 3.4×10^{10} antibodies are required to cover the sensor area. The molecular weight of listeria antibody is 59 kDa (obtained from MSDS sheet), which is equal to 9.797×10^{-20} g. The concentration used in the present work is 0.1 mg/ml, which in turn contains 1.02×10^{15} antibodies. This number of antibodies (1.02×10^{15}) in initial concentration is more

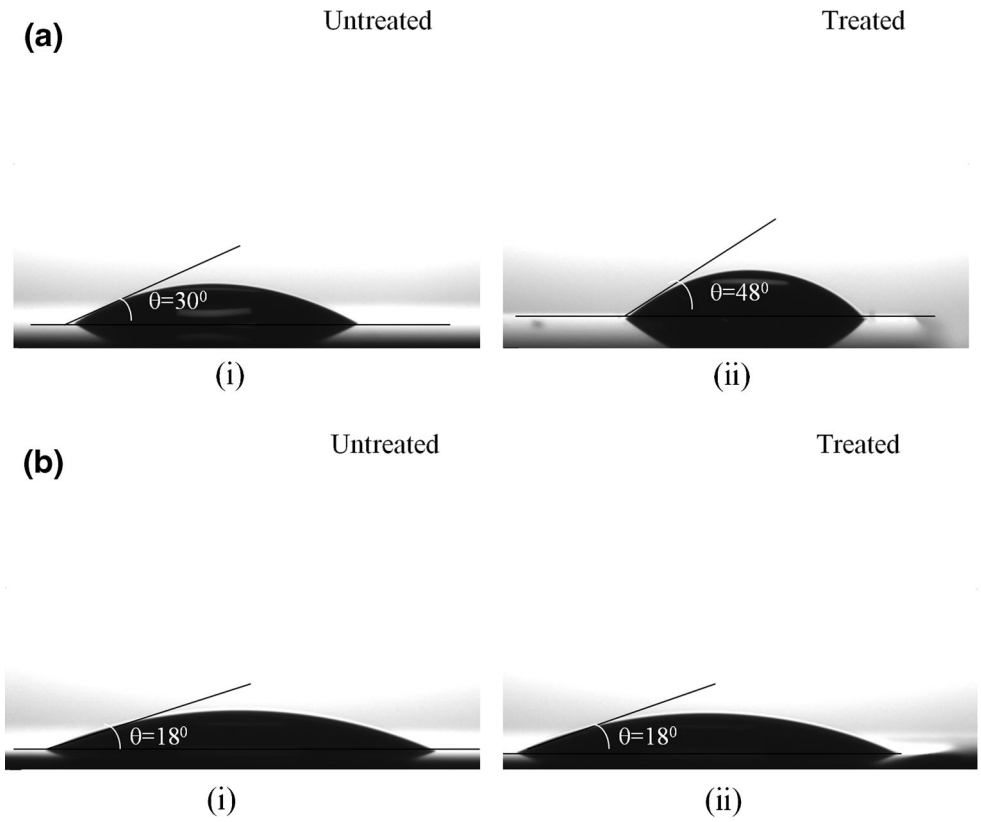

Fig. 4 **a** Contact angle measurements of silicon nitride surface (i) bare and (ii) treated with glutaraldehyde; **b** Contact angle measurements of silicon dioxide surface (i) bare and (ii) treated with glutaraldehyde

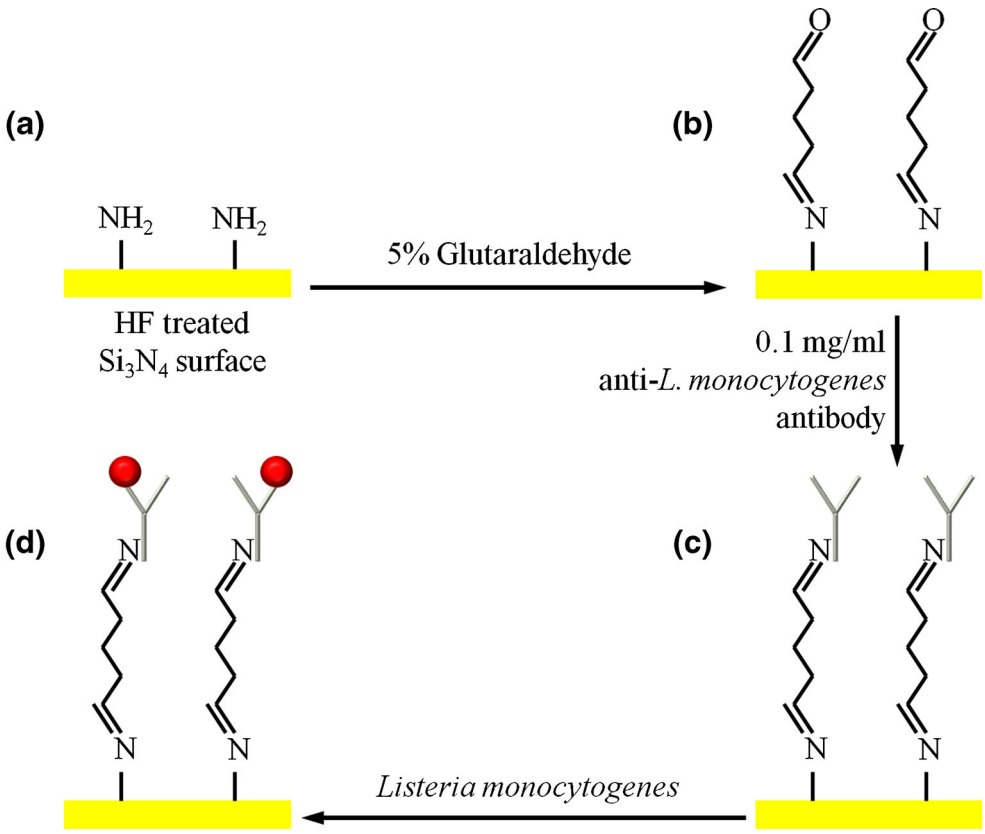

Fig. 5 Schematic representation of immunoassay procedure on silicon nitride sensing area. **a** Amine groups activated by HF on silicon nitride surface, **b** 5 % glutaraldehyde treatment, **c** covalent bonding of antibodies with the aldehyde groups of glutaraldehyde and **d** *Listeria monocytogenes* captured by the antibodies

than sufficient required for sensor area (3.4×10^{10}). Hence, the concentration used in the present work is sufficient to produce a monolayer of antibodies on sensor surface.

To confirm the specificity of the immobilization procedure, FITC tagged rabbit anti-*L. monocytogenes* antibodies (0.1 mg/ml) was added after the last step. After rinsing the surfaces with PBS and blow drying, they were observed under an inverted fluorescence microscope. Figure 6a shows the fluorescent image of the silicon nitride surface whereas Fig. 6b shows the fluorescent image of the silicon dioxide surface. The presence of bacteria only on the silicon nitride surface is clearly visible from these microscopy images, which again confirms the specific binding of *Listeria* to the sensor area.

3.2.4 Scanning electron microscopy

Selectivity of the surface modified MZI chips was analyzed by SEM imaging. Two MZI chips were prepared with glutaraldehyde and antibodies, as described in the previous subsections. One of the chips was incubated with a 10^9 CFU/ml *L. monocytogenes* solution for 30 mins while the other was incubated with a 10^9 CFU/ml *E. coli* solution for 30 mins. After that, both the chips were rinsed with PBS and DI-H_2O but not dried. To preserve the shape of the bacteria for SEM images, the cells are dehydrated in a graded series of ethanol (30 %, 50 %, 70 %, 80 %, 90 %, 96 % and 100 %) and then dried in a critical point drier (CPD). Bacteria contain high proportions of water in their cells and thus, when they are placed in a high vacuum SEM chamber, the water readily evaporates. During evaporation, large surface tension forces are created which lead to the collapse of the bacterial cells. The critical point of a liquid-gas system represents the temperature and pressure above which the phase boundary between the liquid and gas disappears (Heady and Cahn 1973) and thus the devastating effects of surface tension forces cease to exist. However, the critical point of water is quite high (374 °C, 229 bar) and can destroy the bacterial cells. To overcome this problem, water can be replaced by liquid carbon dioxide (LCO_2), whose critical point is at 31 °C and 74 bar and does not damage bacterial samples. The graded ethanol series dehydration was performed prior to the CPD step in order to replace all the water in the bacterial cells with ethanol since LCO_2 is miscible with ethanol and not with water. Finally, during the critical point drying step, the LCO_2 is evaporated by maintaining its critical temperature and decreasing the pressure. The chips are then mounted on an SEM stub and sputter-coated with gold before placing it in the SEM chamber for imaging (Gunda et al. 2013). Figure 7a shows the SEM image of one *L. monocytogenes* bacterial cell with its shape preserved by critical point drying. Figure 7b and c show the SEM images of the sensor area of MZI chips incubated with *E. coli* and *L. monocytogenes*, respectively. These figures clearly show that the MZI chips are selective only to a given species of bacteria (*L. monocytogenes*).

3.3 Power measurements

The MZI chips were polished in a custom made waveguide polisher from Ultratec Manufacturing, Inc. and were placed on a piezo-controlled XYZ stage with a minimum resolution of 20 nm. Light from a He-Ne laser (633 nm) was coupled into the core layer of the chip using a 40X objective lens. The light emanating from the chip was collected by a photodiode. No optical fibers were used in this experiment either to couple the laser light into the chip or collect the light at the output end of the chip. Optical fibers are prone to losses and hence the exclusion of such fibers can increase the efficiency of the device. However, the exclusion of fiber optics makes alignment of the optical components very difficult. For this reason, two complementary metal-oxide-semiconductor (CMOS) cameras have been used for the alignment of the laser-chip system. An overhead camera is placed directly above the chip to monitor the lateral alignment of the laser light into the MZI structure. The

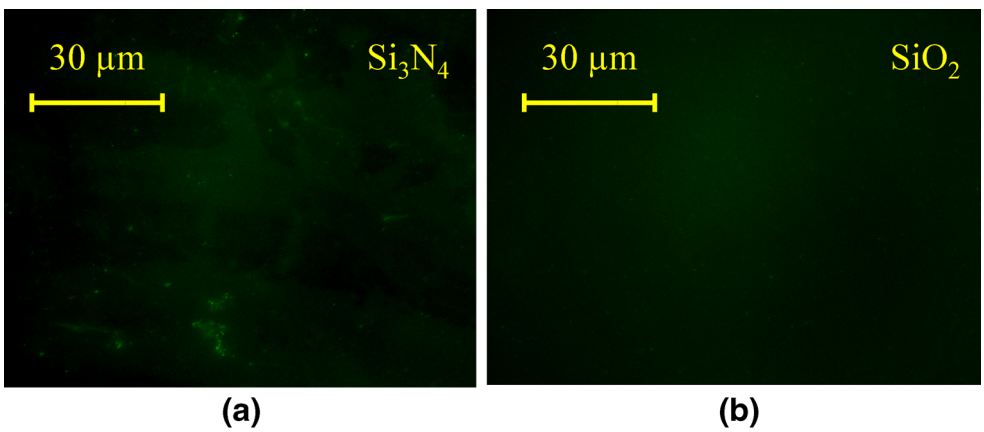

Fig. 6 Fluorescence microscope images of **a** surface treated silicon nitride surface showing bacterial cells and **b** surface treated silicon dioxide surface devoid of bacterial cells

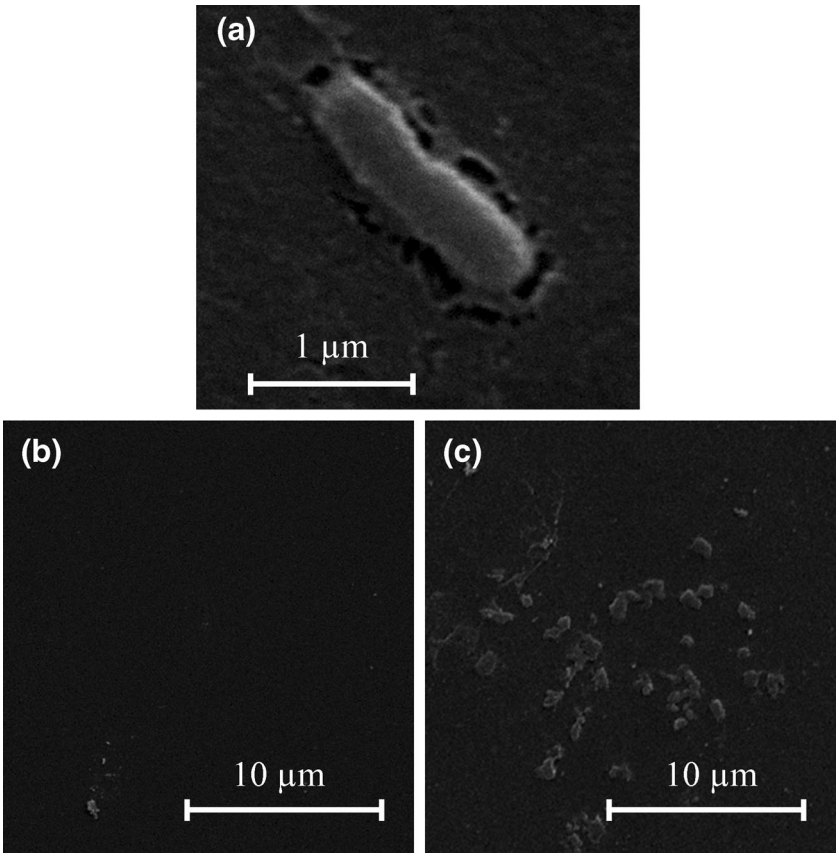

Fig. 7 SEM images of **a** a single rod-shaped *Listeria monocytogenes* cell, **b** sensor area incubated with *E. coli* and **c** sensor area incubated with *L. monocytogenes*

vertical alignment is monitored by another CMOS camera placed at the output end of the chip parallel to the direction of propagation of light. Once the optical system is aligned, the horizontal camera is replaced with a photodiode giving the corresponding power reading through a digital read-out. Details related to the alignment procedure can be found elsewhere (Sarkar et al. 2013).

As mentioned earlier (refer Section 1), the interaction of the biomolecules with the evanescent field of the light waves in the sensor arm of the MZI waveguide causes a change in the effective refractive index of the sensor arm which leads to a phase difference between the sensor and reference arms, given by (Boiarski et al. 1993),

$$\Delta\phi = \frac{2\pi}{\lambda} S_l \Delta N_{eff} \tag{1}$$

where, $\Delta\phi$ is the phase change between the guided light in the sensor and reference arms, λ is the wavelength and ΔN_{eff} is the change in the effective refractive index due to the biointeraction. This phase change, in turn, leads to the change in the normalized power output(ratio of output to input power) of the MZI chip, which can be written as (Boiarski et al. 1993),

$$\Delta P = \frac{1 + cos\Delta\phi}{2} \tag{2}$$

where,

$$\Delta P = \frac{P_{out}}{P_{in}} \tag{3}$$

Here, ΔP is the normalized power output, P_{out} is the output power and P_{in} is the input power of the MZI chip. In this work, we have calculated the normalized power output values for different concentrations of *Listeria* varying from 2.8×10^3 to 2.8×10^{13} CFU/ml by performing power measurements at the input and output end of the MZI chips.

4 Results and discussion

Fabrication, surface modification, and biofunctionalization of *S*3 MZI chips were carried out according to the procedure mentioned in the previous sections. Prior to power measurements with bacteria, a negative control was introduced in order to verify that the change in signal was indeed only due to the immobilization of bacteria on the MZI chip. The negative control implies that power measurements were taken after the antibody binding step and before the *L. monocytogenes* biofunctionalization. This was done for every MZI chip used in the experiments and it gave a constant reading (refer Fig. 8). Note that, we repeated the experiments for

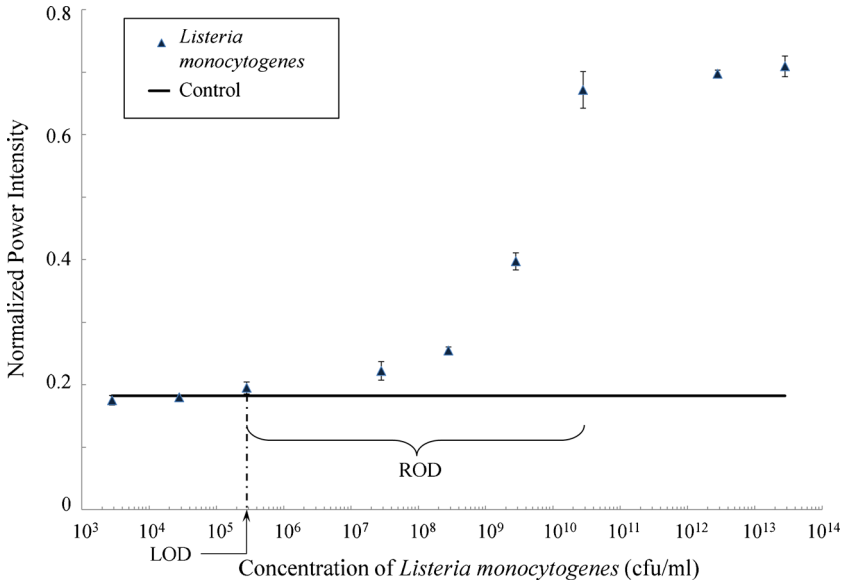

Fig. 8 Variation of output power with increase in concentration of *Listeria*. The control represents the output power of the biosensor after the antibody bonding step and before the *L. monocytogenes* biofunctionalization

three times for all the concentrations and for all the cases (single and mixed dilutions of bacterial pathogens).

Figure 8 illustrates the variation in the normalized power output of the chip with change in concentration of *L. monocytogenes*. It can be seen that the normalized power intensity increases with the increase in microbial concentration. In general, a higher concentration of bacteria would result in a better surface coverage of the sensor area.

Figure 8 also reveals that the output power has a significant intensity as compared to the control even when the bacterial concentration is as low as 2.8×10^5 CFU/ml, which is well below the infective dosage of *L. monocytogenes* for healthy human beings. On decreasing the concentration even further, no significant power intensity was detected. Therefore, the limit of detection (LOD) for this biosensor is in the order of 10^5 CFU/ml. The LOD of this device has the potential to be of much lower value by using better quality antibodies as it has been reported by others that the quality of antibodies highly affects the sensitivity of the biosensor (Tims et al. 2001). The LOD obtained in this work is better than the LOD achieved by most of the alternative methods. Koubov et al. (2001) demonstrated the detection of heat-killed *Listeria* using a physically adsorbed antibody crosslnked with glutaraldehyde. The LOD of their method was 10^6 CFU/ml. Leonard et al. (2004) detected the heat-killed *Listeria* using inhibition assay with a Biacore 3000 surface plasmon resonance (SPR) spectrometer. The LOD of their method was 10^5 CFU/ml. Hearty et al. (2006) produced novel monoclonal antibodies specific to *Listeria* and demonstrated the detection of listeria using Biacore 3000 SPR spectrometer. The LOD achieved with novel antibodies was 10^7 CFU/ml. Rowe et al. (1999) developed a fluorescence planar waveguide to demonstrate the sandwich immunoassay to detect *Listeria* in buffer solution. They achieved a LOD of 10^6 CFU/ml. Geng et al. (2004) detected *Listeria* up to 4.3×10^3 CFU/ml in hot dog and bologna using Analyte 2000. In context to the level of *Listeria* found in food samples, which is often more than 10^6 CFU/ml as in case of chocolate milk (Dalton et al. 1997), it further confirms that our detection mechanism will able to detect such occurrence of contamination in food samples.

Another important parameter that has been used to characterize this biosensor is its range of detection (ROD). From Fig. 8, it is evident that beyond 2.8×10^{10} CFU/ml, the normalized power intensity value is invariant to the change in *L. monocytogenes* concentration. This can be attributed to the fact that at high concentrations of *L. monocytogenes*, complete coverage of the sensor area takes place and the addition of any further amount of analytes would not enhance the signal. In other words, the biosensor is said to be saturated. In this case, the MZI biosensor has reached its saturation at 10^{10} CFU/ml concentration of *L. monocytogenes*. Hence the ROD of this device is from 10^5 CFU/ml to 10^{10} CFU/ml.

In order to determine the selectivity of the MZI biosensor, similar power measurement tests were performed on *S*3 MZI chips with *Escherichia coli*. All surface modification steps were kept the same except for the *L. monocytogenes* immobilization step. Instead, two different batches of bacterial solutions were added on separate MZI chips. One batch of solutions contained *E. coli* with concentrations varying between 10^5 CFU/ml and 10^{10} CFU/ml while the other batch contained a mixture of *L. monocytogenes* and *E. coli* (1:1 by volume). The latter batch is prepared by mixing a fixed concentration of E. coli (10^9 CFU/ml.) with varying concentrations of L. monocytogenes (2.8×10^5 CFU/ml—2.8×10^9 CFU/ml) Fig. 9 illustrates the variation of normalized power intensity with the change in concentration of *E. coli* and the mixture of *E. coli* and *L. monocytogenes*,

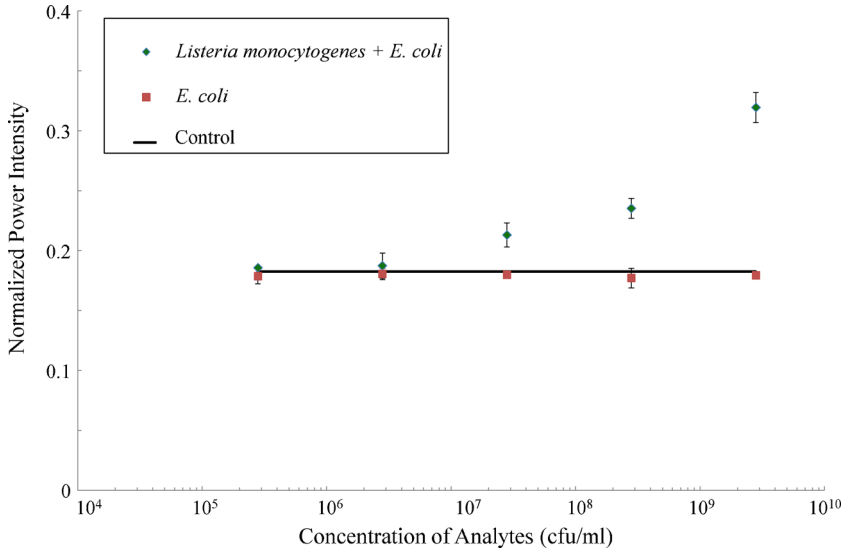

Fig. 9 Variation of output power with increase in concentration of analytes. The *red squares* indicate only *E. coli* in the analyte solution for which the horizontal axis represents the concentration of *E. coli*. The *green diamond shapes* indicate mixture of *E. coli* and *L. monocytogenes* in 1:1 ratio for which the horizontal axis represents the concentration of *Listeria*

respectively. It can be seen that the *E. coli* alone does not produce any power signal above the control whereas the *L. monocytogenes* and *E. coli* mixture produces a detectable power, which exceeds the control. However, MZI chips containing a mixture of *L. monocytogenes* and *E. coli* showed lower values of ΔP compared to the MZI chips containing only *L.monocytogenes* for the same values of concentration of *Listeria* (see Figs. 8 and 9). This was due to the dilution caused by the *E. coli* solution. Another probable reason may be the interference in binding of *L. monocytogenes* cells due to presence of *E. coli*. However, these results clearly show that the output signal is due to *L. monocytogenes* alone and that the fabricated MZI biosensor is highly selective to *L. monocytogenes*.

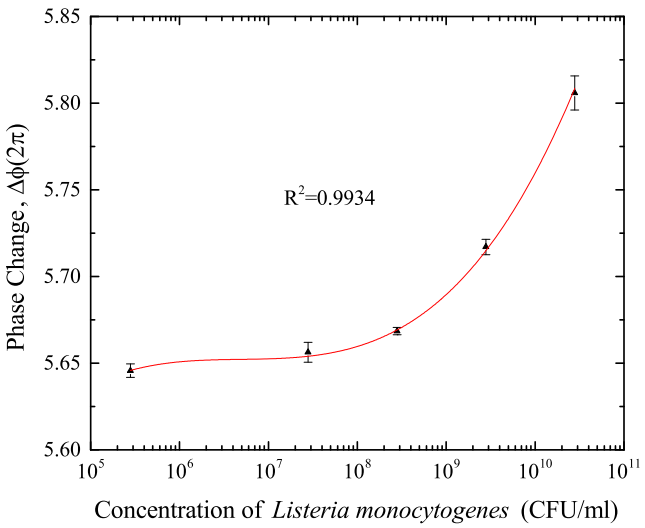

Fig. 10 Variation of phase change, calculated from Eq. 2 for a known value of ΔP, with increase in concentration of *Listeria* within the range of detection (ROD)

Figure 10 represents the variation of phase change, calculated from Eq. 2 for a known value of ΔP, with the change in concentration of *L. monocytogenes* within the range of detection. A third order polynomial fit to the data points ($R^2 = 0.9934$) is done. It provides the variation of the phase change with respect to concentration of *L. monocytogenes*. This can be used as a calibration curve for the MZI chip and can therefore be used as a guide to estimate the value of an unknown concentration of *L. monocytogenes* in a given sample from its phase change value obtained from experiments.

5 Conclusion

In this paper, we have demonstrated a Mach-Zehnder Interferometer with the capability to detect *Listeria monocytogenes*. Ten different MZI Y-junction designs were investigated and an optimum design (*S3*) with a large sensor area (1.5 mm^2) and low optical losses (0.4 dB/cm) was chosen for experiments. A specific biofunctionalization protocol was used where, surface treatment of silicon nitride surface with HF greatly reduced the time of antigen immobilization as compared to other traditional methods which use 3-Aminopropyl triethoxysilane (APTES) to create amine groups on the surface. SEM analysis of MZI chips incubated with *L. monocytogenes* and *E. coli* demonstrated the selectivity of the biosensor to *L. monocytogenes*. Power measurements were performed to determine the limit of detection (LOD) and range of detection (ROD) of the fabricated MZI. The LOD of the device is in the order of 10^5 CFU/ml, which is lower than the infection dosage of *Listeria* for healthy human beings. Experimental results also showed that the normalized power output of the MZI biosensors increased with the increase in concentration of

the *L. monocytogenes* microbial solution, however, addition of *E. coli* had no such effect confirming the high selectivity of the device to *L. monocytogenes*. Finally, the MZI biosensor was calibrated using phase change data, which can be used to determine unknown concentrations of *L. monocytogenes*. With further developments, this MZI biosensor could be utilized in real-time detection of *L. monocytogenes* directly from ready-to-eat food products available in the market.

Acknowledgments The authors gratefully acknowledge the financial support from Natural Sciences and Engineering Council-Collaborative Research and Development (NSERC-CRD) program and AQL Management Consulting, Inc. We also gratefully acknowledge the useful discussions with Stefania Dante, PhD student at Research Center on Nanoscience and Nanotechnology(CIN2), Spanish National Research Council (CSIC), Barcelona, Spain.

References

C. Almeida, N.F. Azevedo, S. Santos, C.W. Keevil, M.J. Vieira, Discriminating multi-species populations in biofilms with peptide nucleic acid fluorescence *in situ* hybridization (pna fish). PLoS One **6**(3), e14786 (2011)

P. Aureli, G.C. Fiorucci, D. Caroli, G. Marchiaro, O. Novara, L. Leone, S. Salmaso, An outbreak of febrile gastroenteritis associated with corn contaminated by listeria monocytogenes. N. Engl. J. Med. **342**(17), 1236–1241 (2000)

M.-J. Bañuls, V. González-Pedro, C.A. Barrios, R. Puchades, Á. Maquieira, Selective chemical modification of silicon nitride/silicon oxide nanostructures to develop label-free biosensors. Biosens. Bioelectron. **25**(6), 1460–1466 (2010)

A.A. Boiarski, J.R. Busch, B.S. Bhullar, R.W. Ridgway, V.E. Wood, Integrated Optic Sensor with Macro-Flow Cell. *Fibers' 92* (International Society for Optics and Photonics, 1993), pp. 199–211

F. Brosinger, H. Freimuth, M. Lacher, W. Ehrfeld, E. Gedig, A. Katerkamp, F. Spener, K. Cammann, A label-free affinity sensor with compensation of unspecific protein interaction by a highly sensitive integrated optical Mach-Zehnder Interferometer on silicon. Sensors Actuators B Chem. **44**(1–3), 350–355 (1997)

R. Bruck, E. Melnik, P. Muellner, R. Hainberger, M. Lämmerhofer, Integrated polymer-based Mach-Zehnder Interferometer label-free streptavidin biosensor compatible with injection molding. Biosens. Bioelectron. **26**(9), 3832–3837 (2011)

F. Cattaruzza, A. Cricenti, A. Flamini, M. Girasole, G. Longo, A. Mezzi, T. Prosperi, Carboxylic acid terminated monolayer formation on crystalline silicon and silicon nitride surfaces. a surface coverage determination with a fluorescent probe in solution. J. Mater. Chem. **14**(9), 1461–1468 (2004)

C.D. Chin, V. Linder, S.K. Sia, Lab-on-a-chip devices for global health: past studies and future opportunities. Lab Chip. **7**(1), 41–57 (2007)

C.B. Dalton, C.C. Austin, J. Sobel, P.S. Hayes, W.F. Bibb, L.M. Graves, P.M. Griffin, An outbreak of gastroenteritis and fever due to Listeria monocytogenes in milk. N. Engl. J. Med. **336**(2), 100–106 (1997)

C.W. Donnelly, Listeria monocytogenes: a continuing challenge. Nutr. Rev. **59**(6), 183–194 (2001)

P.K.B. Embarek, Presence, detection and growth of Listeria monocytogenesin seafoods: a review. Int. J. Food Microbiol. **23**(1), 17–34 (1994)

D. Esinenco, S. Psoma, M. Kusko, A. Schneider, R. Muller, Su-8 micro-biosensor based on Mach-Zehnder Interferometer. Rev. Adv. Mater. Sci. **10**(4), 295–299 (2005)

X. Fan, I.M. White, S.I. Shopova, H. Zhu, J.D. Suter, Y. Sun, Sensitive optical biosensors for unlabeled targets: a review. Anal. Chim. Acta. **620**(1), 8–26 (2008)

D.M. Frye, R. Zweig, J. Sturgeon, M. Tormey, M. LeCavalier, I. Lee, L. Lawani, L. Mascola, An outbreak of febrile gastroenteritis associated with delicatessen meat contaminated with listeria monocytogenes. Clin. Infect. Dis. **35**(8), 943–949 (2002)

I. Fuchizawa, S. Shimizu, M. Ootsubo, Y. Kawai, K. Yamazaki, Specific and rapid quantification of viable listeria monocytogenes using fluorescence *in situ* hybridization in combination with filter cultivation. Microbes Environ./JSME. **24**(3), 273–275 (2009)

T. Geng, M.T. Morgan, A.K. Bhunia, Detection of low levels of Listeria monocytogenes cells by using a fiber-optic immunosensor. Appl. Environ. Microbiol. **70**, 6138–6146 (2004)

D. Griffiths, G. Hall, Biosensors–what real progress is being made Trends Biotechnol. **11**(4), 122–130 (1993)

N.S.K. Gunda, M. Singh, Y. Purwar, S.L. Shah, K. Kaur, S.K. Mitra, Micro-spot with integrated pillars (MSIP) for detection of dengue virus NS1. Biomed. Microdevices (2013). doi:10.1007/s10544-013-9787-3

R. Heady, J. Cahn, Experimental test of classical nucleation theory in a liquid-liquid miscibility gap system. J. Chem. Phys. **58**, 896 (1973)

R. Heideman, P. Lambeck, Remote opto-chemical sensing with extreme sensitivity: design, fabrication and performance of a pigtailed integrated optical phase-modulated mach–zehnder interferometer system. Sensors Actuators B Chem. **61**(1), 100–127 (1999)

R. Heideman, R. Kooyman, J. Greve, Performance of a highly sensitive optical waveguide Mach-Zehnder Interferometer immunosensor. Sensors Actuators B Chem. **10**(3), 209–217 (1993)

S. Hearty, P. Leonard, J. Quinn, R. Oennedy, Production, characterisation and potential application of a novel monoclonal antibody for rapid identification of virulent Listeria monocytogenes. J. Microbiol. Methods. **66**, 294–312 (2006)

D. Ivnitski, I. Abdel-Hamid, P. Atanasov, E. Wilkins, Biosensors for detection of pathogenic bacteria. Biosens. Bioelectron. **14**(7), 599–624 (1999)

M. Karymov, A. Kruchinin, Y.A. Tarantov, I. Balova, L. Remisova, Y.G. Vlasov, Fixation of dna directly on optical waveguide surfaces for molecular probe biosensor development. Sensors Actuators B Chem. **29**(1), 324–327 (1995)

H.-J. Kim, J.-C. Cho, Simple and rapid detection of Listeria monocytogenes in fruit juice by real-time pcr without enrichment culture. Food Control. **21**(10), 1419–1423 (2010)

P. Kotzekidou, Survey of listeria monocytogenes, salmonella spp. and escherichia coli o157:h7 in raw ingredients and ready-to-eat products by commercial real-time pcr kits. Food Microbiol. **35**(2), 86–91 (2013)

V. Koubov, E. Brynda, L. Karasov, J. Kvor, J. Homola, J. Dostlek, P. Tobika, J. Roick, Detection of foodborne pathogens using surface plasmon resonance biosensors. Sensors Actuators B Chem. **74**, 100–105 (2001)

P. Leonard, S. Hearty, J. Brennan, L. Dunne, J. Quinn, T. Chakraborty, R. OKennedy, Advances in biosensors for detection of pathogens in food and water. Enzym. Microb. Technol. **32**(1), 3–13 (2003)

P. Leonard, S. Hearty, J. Quinn, R. Oennedy, A generic approach for the detection of whole Listeria monocytogenes cells in contaminated samples using surface plasmon resonance. Biosens. Bioelectron. **19**, 1331–1335 (2004)

P. MacDonald, R. Whitwam, J. Boggs, J. Reardon, R. Saah, M. Beatty, J. Sobel, L. Graves, S. Hunter, J. MacCormack, in *Clinical Infectious Diseases.* Outbreak of Listeria-Associated Birth Complications Linked with Homemade Mexican-Style Cheese, North Carolina, 2000, vol. 33 (Univ Chicago Press, Chicago, 2001), pp. 1236–1236

M. Marazuela, M. Moreno-Bondi, Fiber-optic biosensors–an overview. Anal. Bioanal. Chem. **372**(5–6), 664–682 (2002)

J. Mattingly, B. Butman, M. Plank, R. Durham, B. Robison et al., Rapid monoclonal antibody-based enzyme-linked immunosorbent assay for detection of listeria in food products. J. Assoc. Off. Anal. Chem. **71**(3), 679–681 (1987)

V. Menon, R. Donovan, *Handbook of Semiconductor Wafer Cleaning Technology* (Noyes Publication, New Jersey, 1993)

Y. Moreno, L. Ballesteros, J. García-Hernández, P. Santiago, A. González, M.A. Ferrús, Specific detection of viable Listeria monocytogenes in spanish wastewater treatment plants by fluorescent *in situ* hybridization and pcr. Water Res. **45**(15), 4634–4640 (2011)

R. Müller, P. Obreja, M. Kusko, D. Esinenco, C. Tibeica, G. Conache, L. Buia, D. Apostol, V. Damian, M. Mateescu, et al., in *Advanced Topics in Optoelectronics, Microelectronics, and Nanotechnologies II.* Su 8 used as Optical Waveguide in Integrated Optical Microsensor for Biological Applications (International Society for Optics and Photonics, 2005) pp. 59720Z–59720Z

E. Omiccioli, G. Amagliani, G. Brandi, M. Magnani, A new platform for real-time pcr detection of *Salmonella* spp., *Listeria monocytogenes* and *Escherichia coli* o157 in milk. Food Microbiol. **26**(6), 615–622 (2009)

B.P. Pal, *Fundamentals of Fibre Optics in Telecommunication and Sensor Systems* (Bohem Press, 1992)

O. Parriaux, G. Veldhuis, Normalized analysis for the sensitivity optimization of integrated optical evanescent-wave sensors. J. Light. Technol. **16**(4), 573–582 (1998)

J. Pochop, M. Kačániová, L. Hleba, L. Lopasovskỳ, A. Bobková, L. Zeleňáková, M. Stričík, Detection of listeria monocytogenes in ready-to-eat food by step one real-time polymerase chain reaction. J. Environ. Sci. Health B **47**(3), 212–216 (2012)

A. Rohrbach, Observing secretory granules with a multiangle evanescent wave microscope. Biophys. J. **78**(5), 2641–2654 (2000)

C.A. Rowe, S.B. Scruggs, M.J. Feldstein, J.P. Golden, F.S. Ligler, An array immunosensor for simultaneous detection of clinical analytes. Anal. Chem. **71**, 433–439 (1999)

D. Sarkar, I. Jamal, S.K. Mitra, Analysis, design and fabrication of optical waveguides for mach-zehnder interferometry. Opt. Commun. **311**, 338–345 (2013)

W.F. Schlech, D. Acheson, Foodborne listeriosis. Clin. Infect. Dis. **31**(3), 770–775 (2000)

B. Sepulveda, J.S. Del Rio, M. Moreno, F. Blanco, K. Mayora, C. Domínguez, L.M. Lechuga, Optical biosensor microsystems based on the integration of highly sensitive Mach–Zehnder Interferometer devices. J. Opt. A Pure Appl. Opt. **8**(7), S561 (2006)

A. Sewell, D. Warburton, A. Boville, E. Daley, K. Mullen, The development of an efficient and rapid enzyme linked fluorescent assay method for the detection of Listeria spp. from foods. Int. J. Food Microbiol. **81**(2), 123–129 (2003)

B. Shu, C. Zhang, D. Xing, Highly sensitive identification of foodborne pathogenic listeria monocytogenes using single-phase continuous-flow nested pcr microfluidics with on-line fluorescence detection. Microfluid. Nanofluid. **15**(2), 161–172 (2013)

L. Su, W. Jia, C. Hou, Y. Lei, Microbial biosensors: a review. Biosens. Bioelectron. **26**(5), 1788–1799 (2011)

T.B. Tims, S.S. Dickey, D.R. Demarco, D.V. Lim, Detection of low levels of listeria monocytogenes within 20 hours using an evanescent wave biosensor. Am. Clin. Lab. **20**(8), 28–31 (2001)

U. Traunšek, N. Toplak, B. Jeršek, A. Lapanje, T. Majstorović, M. Kovač, Novel cost-efficient real-time pcr assays for detection and quantitation of Listeria monocytogenes. J. Microbiol. Methods. **85**(1), 40–46 (2011)

S. Ueda, Y. Kuwabara, Evaluation of an enzyme-linked fluorescent assay for the detection of listeria monocytogenes from food. Biocontrol Sci. **15**(3), 91–95 (2010)

K.R. Williams, R.S. Muller, Etch rates for micromachining processing. J. Microelectromech. Syst. **5**(4), 256–269 (1996)

K. Zinoviev, L.G. Carrascosa, J. Sánchez del Río, B. Sepúlveda, C. Domínguez, L.M. Lechuga, in *Advances in Optical Technologies, 2008.* Silicon Photonic Biosensors for Lab-on-a-chip Applications (2008)